Applied Geochemistry 162 (2024) 105900

Contents lists available at ScienceDirect

Applied Geochemistry

journal homepage: www.elsevier.com/locate/apgeochem

Phosphonate functionalized magnetic mesoporous silica for rare earth element recovery from citrate assisted solid waste extracts

Dien Li [a], Yinghao Wen [b], Lei Hu [b], Xiaoyu Xu [c], Breann S. Spencer [c], Shani Egodawatte [d], Sarah C. Larsen [e], Yuanzhi Tang [b,*]

[a] Savannah River National Laboratory, Aiken, SC, 29808, USA
[b] School of Earth and Atmospheric Sciences, Georgia Institute of Technology, Atlanta, GA, 30332, USA
[c] Savannah River Ecology Laboratory, University of Georgia, Aiken, SC, 29802, USA
[d] Department of Chemistry, University of Iowa, Iowa City, IA, 52242, USA
[e] Department of Chemistry, University of Houston, Houston, TX, 77204-5003, USA

ARTICLE INFO

Editorial handling by Dr. Zimeng Wang

Keywords:
REE recovery
Phosphonate functionalization
Magnetic mesoporous silica
Citrate-assisted extraction
Municipal solid waste incineration ashes

ABSTRACT

The growing high demand of rare earth elements (REEs) has prompted extensive research on REE recovery from waste streams. This study reports the synthesis and evaluation of phosphonate-functionalized magnetic mesoporous silica (MMS-PP) for REE recovery from the acidic extracts of solid wastes. MMS-PP was synthesized using surfactant template and post-synthesis methods, and tested using simulated and real extraction solutions from citrate-assisted REE extracts from municipal solid waste incineration (MSWI) ash. The organic-inorganic hybrid MMS-PP was evaluated for La recovery from 50 mM simulated citrate extract, with the adsorption capacity of 13.5 mg/g compared to ~2.5 mg/g for non-functionalized MMS. The MMS-PP material exhibited fast adsorption within 10 min, good La selectivity against competing Na^+ and Ca^{2+}, moderate selectivity against Al^{3+} and Fe^{3+}, high recyclability over multiple adsorption-desorption cycles, and equivalent efficiency for La, Ce, Nd, and Y recovery. The MMS-PP material also demonstrated 70–95% REE recovery from real citrate extracts of MSWI ash, and the spent MMS-PP material can be regenerated and reused for multiple cycles. Functionalized mesoporous materials in combination with organic-ligand assisted extraction can potentially provide a green, effective, and tunable solid-liquid separation platform for REE recovery from complex solid waste streams.

1. Introduction

Rare earth elements (REEs) are a group of critical metals that are used in a wide range of industries and clean energy technologies (Daigle and DeCarlo, 2021). With the rapidly increasing demand and potential geopolitical conflicts due to imbalanced resource distribution, it is critical to seek new alternative and sustainable resources to secure domestic REE supply. Along this direction, REE recovery from various waste sources have been explored, such as industrial, electronic, and municipal wastes, some of which contain reasonably high REE content and may offer unique opportunities for REE recovery (Hsu et al., 2019). In addition to resource exploration, it is highly desirable to develop green and sustainable technologies for REE and other critical metal recovery from waste streams with high efficiencies and low environmental impacts. Mineral acids (*i.e.*, HNO_3, HCl, and H_2SO_4) are commonly used for extracting REEs from solid wastes (Honaker et al., 2019), but they tend to generate large amounts of highly acidic waste byproducts and pose environmental and health hazards. To minimize environmental impacts during REE extraction, research has been directed to the use of organic acids (Gergoric et al., 2018; Lazo et al., 2018) or microbially mediated processes (Auerbach et al., 2019; Brewer et al., 2019), which have shown comparable extraction efficiency to mineral acids under less harsh pH conditions (Antonick et al., 2019). Our recent study used a citrate-assisted method for the extraction of REE from coal fly ash (Liu et al., 2023) and municipal solid waste incineration (MSWI) ash (Wen et al., 2023.), which achieved high REE extraction efficiency under mild pH of ~4.

Following the leaching step, REEs can be recovered, concentrated, and separated from the acidic leachates using various conventional solvent extraction methods (Smith et al., 2019; Wu et al., 2018). Ionic liquids (Huang et al., 2019; Makanyire et al., 2016) and membrane solvent extraction (Smith et al., 2019; Kim et al., 2015) have been

* Corresponding author.
E-mail address: yuanzhi.tang@eas.gatech.edu (Y. Tang).

https://doi.org/10.1016/j.apgeochem.2024.105900
Received 7 August 2023; Received in revised form 16 December 2023; Accepted 4 January 2024
Available online 5 January 2024

proposed as alternatives to conventional solvent extraction. While these methods demonstrated some advantages (*e.g.*, negligible vapor pressure, non-flammability, and decreased non-aqueous solvent use), they also suffer from several drawbacks such as high cost, slow mass transport, and difficulty in REE stripping. Solid-liquid extraction can potentially overcome the shortcomings associated with solvent extraction (*i.e.*, high cost, low REE recovery rate, and toxic liquid/solid wastes), especially with the development of functionalized sorbents such as mesoporous silica materials. Mesoporous silica is a form of silicon dioxide with large and tunable pores by size and geometry. The pores can be readily functionalized with organic ligands (Fryxell et al., 2007), which can significantly enhance the effective and selective sequestration of various metals from aqueous media (Fryxell et al., 2005). Mesoporous silica materials functionalized with several amine-, carboxyl-, and phosphonate-type ligands have been tested for REE recovery from aqueous media (Ravi et al., 2018a; Salih et al., 2021; Hu et al., 2017, 2019; Florek et al., 2014, 2015; Ma et al., 2014; Zheng et al., 2015, 2020a; Yantasee et al., 2009; Liu et al., 2019; Yin et al., 2020; Lee et al., 2019; Ramasamy et al., 2017; Zhang et al., 2017; Callura et al., 2018). These systems demonstrated improved REE recovery efficacy under acidic to circumneutral conditions. Mesoporous silica material can be further tailored to incorporate a magnetic core for easy operation and extraction. Indeed, magnetic mesoporous silica (MMS) has recently been applied to the removal and magnetic separation of heavy metals (primarily CrO_4^{2-} and U(VI)) from contaminated aqueous media (Egodawatte et al., 2015; Li et al., 2016; Chen et al., 2011; Zhang et al., 2012; Zhao et al., 2014), but no studies have investigated the use of functionalized MMS for REE separation from organic-ligand containing extracts.

The goal of this study is to design and evaluate molecular mesoporous materials for effective REE recovery from organic ligand-assisted extracts of solid wastes. We developed a phosphonate-functionalized MMS (MMS-PP) material, and evaluated its performance on REE recovery from a citrate-assisted extraction simulant and a real MSWI ash leachateGutiérrez-Gutiérrez et al., 2015. Benefits of this MMS-PP materials include that: (1) the magnetic core can provide the benefits of easy particle retrieval via magnetic separation; (2) the mesoporous silica has high surface areas and more active sites leading to high REE adsorption capacity; and (3) the functionalized phosphonate ligand can improve REE selectivity from complex chemistry solutions. The synthesized MMS-PP material was characterized using high and small angle powder X-ray diffraction (XRD), N_2 adsorption-desorption isotherms, ^{13}C and ^{31}P cross-polarization magic-angle-spinning nuclear magnetic resonance (CPMAS NMR) spectroscopy. The MMS-PP material, in comparison with non-functionalized MMS, was evaluated for La recovery from deionized (DI) water and 50 mM citric acid extraction simulant. The maximum La adsorption capacity and the effects of reaction time, solid/liquid ratio, citrate concentration, competing cations (*i.e.*, Na, Ca, Al and Fe), and adsorption-desorption cycles were investigated. In addition, the MMS-PP material was demonstrated for effective REEs recovery from a real citrate assisted extraction solution of MSWI ash.

2. Experimental section

2.1. Materials and chemicals

ACS grade or higher chemicals were purchased from Sigma Aldrich (St. Louis, USA), Fisher Scientific (Waltham, USA), and Alfa Aesar (Haverhill, USA). All chemicals were used as received. Deionized (DI) water was used as the solvent for all solutions in this study unless mentioned otherwise.

2.2. Synthesis of MMS material

Magnetite Fe_3O_4 was synthesized using a previous reported method (Lin and Haynes, 2009). 4.8 g ferric chloride and 2.0 g ferrous chloride were dissolved in 30 mL DI water, and the solution was stirred under nitrogen atmosphere at 90 °C on a hot plate. 20 mL NH_4OH solution was added to precipitate Fe_3O_4, and the suspension was aged for 2.5 h, vacuum filtered, washed with DI water, and dried at 100 °C. Next, MMS material was synthesized using an approach previously described for mesoporous silica (MCM-41) synthesis, (Egodawatte et al., 2015; Knezevic et al., 2012) in the presence of Fe_3O_4 nanoparticles. Typically, 1 g cetyltrimethylammonium bromide (CTAB), 3.5 mL of 2 M NaOH, and 500 mL DI water were mixed with 300 mg Fe_3O_4 and sonicated. The solution was heated at 80 °C on a hot plate and tetraethoxysilane was added. The reaction mixture was aged for 2 h and vacuum filtered, washed with DI water and methanol, and dried at 120 °C overnight. The CTAB template was removed by calcining the product at 600 °C in flowing compressed air for 6 h to obtain MMS.

2.3. Functionalization of MMS with phosphonate (PP) group

One gram of calcined MMS was refluxed with 3-(trihydroxysilyl) propyl methylphosphonate (4 mmol) in 1,4-dioxane at 100 °C for 4 h. The reaction mixture was vacuum filtered, washed with 1:1 mixture of diethyl ether and dichloromethane, and dried at 100 °C overnight to obtain phosphonate-functionalized MMS (MMS-PP) (Vivero-Escoto et al., 2013). We also synthesized functionalized mesoporous silica (MS-PP) without Fe_3O_4 for NMR characterization, because the Fe_3O_4 in MMS materials interferes with NMR measurements.

We also synthesized a series of other functionalized MMS materials for La recovery from a citrate simulant and REE recovery from a real citrate extract of MSWI ash (**Text S2** and Fig. S1). These materials were prepared using the same MMS substrate material, but with different functional organic ligands (*e.g.*, benzoylthiourea (BT), dihydroimidazole (DIM), polyaryloamidoxime (AD), phosphonate-amino (PPA), poly (propylenimine) (PPI) dendrimer, poly(amidoamine) (PAMAM) dendrimer, or polyethyleneimine (PEI)) (Li et al., 2016). The experimental procedures of functionalizing MMS with other ligands are described in **Text S1**.

2.4. Characterization of MMS-PP

The physical and chemical properties of the calcined MMS and MMS-PP materials were systematically characterized. Powder XRD (Siemens D5000 X-ray diffractometer with Cu Kα and a nickel filter) was used to verify the mesoporous silica and iron oxide structure. High angle patterns (10–80° 2θ, 0.02° step size, 1 s/step) and small angle patterns (1–10° 2θ, 0.02° step size, 1 s/step) were collected. The surface areas, porosity, and pore diameters of the materials were measured using N_2 adsorption on a Nova 1200 Nitrogen Adsorption Instrument (Quantachrome). Calcined MMS and MMS-PP (100 mg) were evacuated overnight at 100 °C and then a 7-point BET isotherm and a 50-point adsorption/desorption isotherm were measured. The data was used for calculating the surface area, pore volume and pore diameter. The pore volume (V_{tot}) and pore diameter were calculated by measuring the amount of adsorbed nitrogen at 0.97 P/P_0 using Barrett-Joyner-Halenda (BJH) analysis. ^{13}C and ^{31}P cross polarization magic angle spinning (CPMAS) NMR experiments were conducted on the functionalized mesoporous silica using a 4 mm rotor and the spinning speed of 10 kHz under a magnetic field of 7T.

2.5. La recovery experiments from simulant solutions

Batch La^{3+} adsorption experiments were conducted at an initial La concentration of 0.5 mM in DI water and 50 mM citric acid extraction simulant under ambient condition. Control experiments were conducted without solid materials. Typically, 0.025 g of MMS or MMS-PP and 2.5 mL solution were added to 15 mL polypropylene centrifuge tubes. La $(NO_3)_3 \bullet 6H_2O$ was used to make a 50 mM La stock solution. After spiking with 0.025 mL of the La stock solution, the suspension was reacted on a

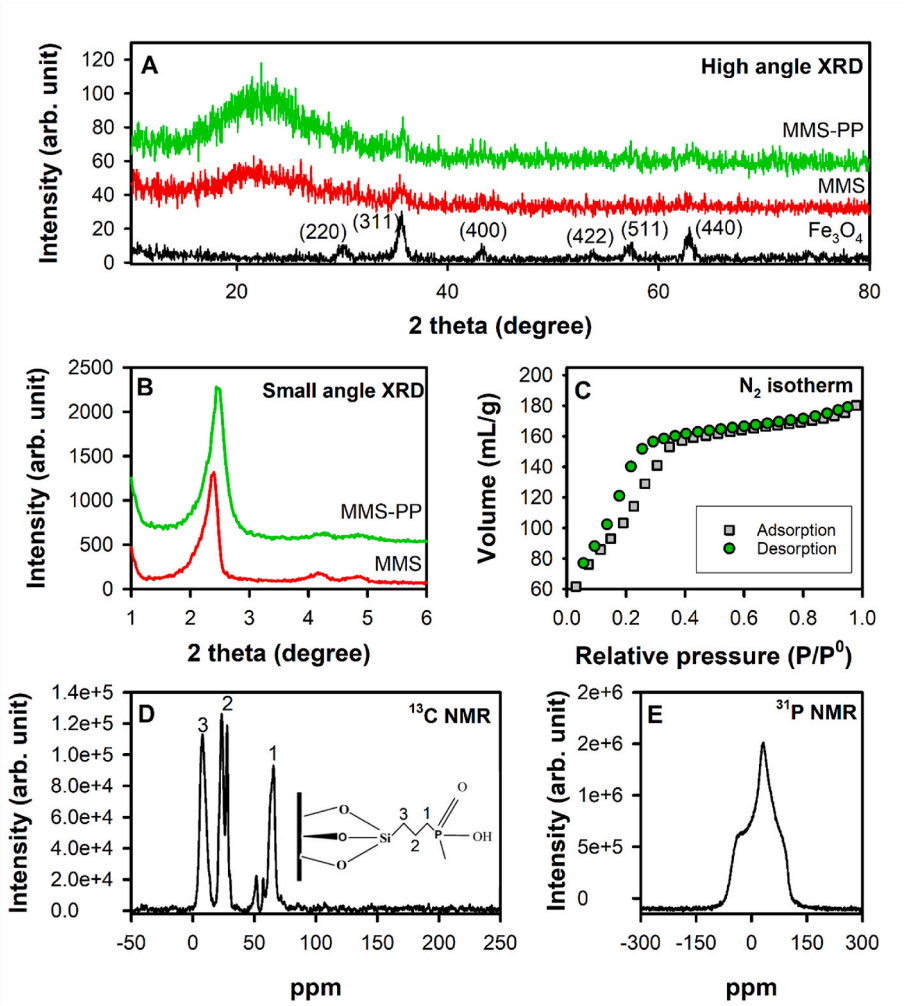

Fig. 1. Characterization of phosphonate-functionalized magnetic mesoporous silica (MMS-PP). **(A)** High angle powder XRD, in comparison with non-functionalized MMS and Fe_3O_4, **(B)** Small angle powder XRD, in comparison with MMS, **(C)** N_2 adsorption-desorption isotherms, **(D)** ^{13}C CPMAS NMR spectrum, **(E)** ^{31}P CPMAS NMR spectrum.

reciprocating shaker for 24 h if not specified. After reaction, each suspension was centrifuged at 10,000 rpm for 10 min and filtered using 0.2 μm polyethersulfone membrane filter. The filtrate was acidified and diluted with 2% HNO_3 and analyzed for La concentration by inductively coupled plasma mass spectrometry (ICP-MS; NexION 300X, PerkinElmer, Inc.). The ICP-MS analysis uncertainty was within ±5%. The La recovery rate and the mass of La sorbed onto the sorbent (q_e, mg/g) were calculated using equations (1) and (2), respectively:

$$Recovery\ rate = \frac{C_{ini} - C_{eq}}{C_{ini}} \times 100 \quad (1)$$

$$q_e = \frac{(C_{ini} - C_{eq}) \times V}{M} \quad (2)$$

where C_{ini} (mg/L) is the initial La concentration in the control samples, C_{eq} (mg/L) is La concentration in the solution at equilibrium, V is the volume of the solution (mL) and M is the mass of the sorbent (g).

In addition, batch experiments for obtaining the adsorption isotherm curves were conducted at initial La concentrations from 0.05 to 5 mM, 0.025 g solid, and 2.5 mL DI water or 50 mM citric acid simulant. The sorption/resorption experiments of MMS-PP were also conducted using 50 mM citric acid simulant with an initial La concentration of 0.5 mM and solid/liquid ratio of 10 g/L, while the La desorption experiment was conducted using 1 M HCl solution.

2.6. REEs recovery from a real MSWI ash extract

Our recent studies (Liu et al., 2023; Wen et al., 2023) developed a method for citrate-assisted REE extraction from coal fly ash and MSWI ash. This method can achieve high REE extraction efficiency at a mild pH of 4. Here we evaluate the performance of MMS-PP material in a real extraction solution, which was obtained from the 106 μm size fraction of a MSWI ash under experimental conditions of liquid/solid ratio 200 mL/g, 50 mM citrate, pH 3.75, 240 rpm, and 4 h. Details of the MSWIA ash and extraction method are in **SI Text S1** and our recent study (Wen et al., 2023). The REEs and major metal concentrations in the extraction solution are in Table S1. The major REEs are Y 7.56 ppb, La 16.18 ppb, Ce 18.71 ppb, Pr 141.22 ppb, Nd 351.77 ppb, and Dy 21.57 ppb. The extraction solution also contains high concentrations of Na, Ca, Al, and Fe at ppm level.

2.7. MMS-PP material recycling and regeneration

To evaluate the regeneration of the MMS-PP material and recovery efficiency of REE from the sorbent, HCl stripping solutions of varied concentration (0.1, 0.5 and 1 M) were evaluated for four-cycle adsorption-desorption experiments. The goal is to minimize HCl use while achieving high efficiency for the material regeneration and REE recycling.

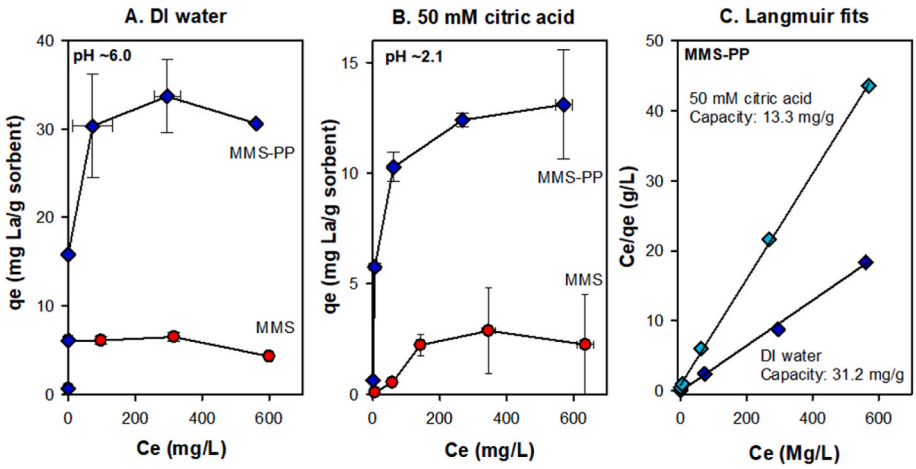

Fig. 2. Adsorption isotherm of La on MMS and MMS-PP. Reaction condition: 24 h, solid/liquid ratio 10 g/L, initial La concentration 0.05–5 mM. **(A)** DI water, **(B)** 50 mM citric acid simulant, **(C)** Langmuir fits to the adsorption isotherm of La on MMS-PP in DI water and 50 mM citric acid simulant.

Table 1
Comparison of REE adsorption capacities on different functionalized mesoporous silica (MS) materials.

REEs	Silica matrix	Functional molecules	Surface area (m^2/g)	Adsorption capacity (mg/g)	pH	Ref.
Ce^{3+}	KIT-6	1,3-tetradentate phenylenedioxy diamide	~550	~11	4	Hu et al. (2019)
	MS	Acetamide phosphonic acid	/	32	2	Yantasee et al. (2009)
Eu^{3+}	KIT-6	Diglycolamide	621	167	4	Florek et al. (2015)
	KIT-6	Dioxaoctanedioic acid	588	149	4	Florek et al. (2015)
Gd^{3+}	MS	Diethylenetriamine	57.4	157.3	5	Salih et al. (2021)
	MCM-41	Maleic anhydride	575	85.4	4	Zheng et al. (2015)
	Hollow MS	Amino-phosphonic acid	825.3	100	2	Yin et al. (2020)
	Hollow MS	Amino-phosphonic acid	825.3	387.3	6	Yin et al. (2020)
	MS foam	Poly(amidoamine) dendrimer	210	38.2	4	Lee et al. (2019)
	MS foam	Poly(amidoamine) dendrimer	210	130.5	6	Lee et al. (2019)
	SBA-15	Inorganic phosphorous acid	669.7	220	4	Gao et al. (2017)
La^{3+}	MS film	Phosphate	300	69.2	7	Liu et al. (2019)
	SBA-15	Phosphoric acid	487	114.8	7	Zheng et al. (2020a)
	MCM-41	Phosphonate	512	31.2	6.0	This work
	MCM-41	Phosphonate	512	13.3	2.1	This work
Lu^{3+}	KIT-6	Bidentate phthaloyl diamide	726	8.6	4	Hu et al. (2017)
Nd^{3+}	MCM-41	n-propy titanium phosphate	443	~47	2.5	Zhang et al. (2017)
	KIT-6	Ethylenediaminetetraacetic acid	334	109.8	6	Ravi et al. (2018b)
	KIT-6	Benzene-1,3,5-triamido-tetraphosphonic acid	276	129.8	6	Ravi et al. (2018a)
	MS	Diethylenetriamine	57.4	124.9	5	Salih et al. (2021)
Pr^{3+}	MS	Diphosphonic acid	/	32	2	Yantasee et al. (2009)
Sc^{3+}	SBA-15	Lysine	223	35.3	5	Ma et al. (2014)

3. Results and discussion

3.1. Characterization of functionalized MMS materials

The high angle powder XRD patterns of MMS, MMS-PP, and Fe_3O_4 in the range of 10–80° 2θ are shown in Fig. 1A. The XRD patterns of both MMS and MMS-PP were characterized with a single broad peak at 20° 2θ, consistent with published XRD pattern for MCM-41 (Kaya et al., 2010). The characteristic peaks for Fe_3O_4 are also present for both MMS and MMS-PP, confirming that Fe_3O_4 nanoparticles are present inside the core-shell particles.

Small angle XRD patterns for MMS and MMS-PP are shown in Fig. 1B. The peak (100) at 2.3° 2θ characterizes the hexagonal ordering of the pores in the MCM-41 framework, which is consistent with published data (Egodawatte et al., 2015). In addition, two weak peaks corresponding to (110) and (200) at 4–5° 2θ were observed for MMS and MMS-PP. The characteristic (100) peak shifted slightly toward higher 2θ, and the (110) and (200) peaks became weaker for MMS-PP relative to MMS, indicating that the functionalized phosphonate molecule was primarily grafted into the mesopores and this functionalization slightly altered the hexagonal ordering of the pores in the MCM-41 framework.

The pore size distributions for MMS and MMS-PP were calculated from the N_2 adsorption isotherms (Fig. 1C) using Barrett-Joyner-Halenda (BJH) analysis. The BET surface area, pore volume, and pore size of MMS were 1010 m^2/g, 0.33 cm^3/g, and 3.3 nm, respectively, while these values were 512 m^2/g, 0.05 cm^3/g, and 3.0 nm for the MMS-PP material, respectively. The pore volumes and sizes calculated using standard BJH method gave average values for all pores. The pore size distribution for the MMS materials calculated using the BJH method was consistent with previously reported values on similar magnetic iron oxide/mesoporous silica nanoparticles (Egodawatte et al., 2015; Knezevic et al., 2012). Compared to MMS, the surface area and pore volume of MMS-PP decreased significantly, suggesting that the functionalized molecules were primarily grafted into the mesopores (~3 nm) and less onto external surfaces of MMS, consistent with previous studies (Egodawatte et al., 2015; Datt et al., 2012). However, the pore size essentially remained unchanged (Egodawatte et al., 2015).

The functionalized mesoporous silica (MMS-PP) without Fe_3O_4 was analyzed by ^{13}C and ^{31}P CPMAS NMR because Fe_3O_4 in MMS materials interferes with NMR measurements. The ^{13}C CPMAS NMR spectrum of MMS-PP is shown in Fig. 1D. The peak at 65.5 ppm chemical shift corresponds to carbon 1 (C-O), the peak at 23.3 ppm is attributed to carbon

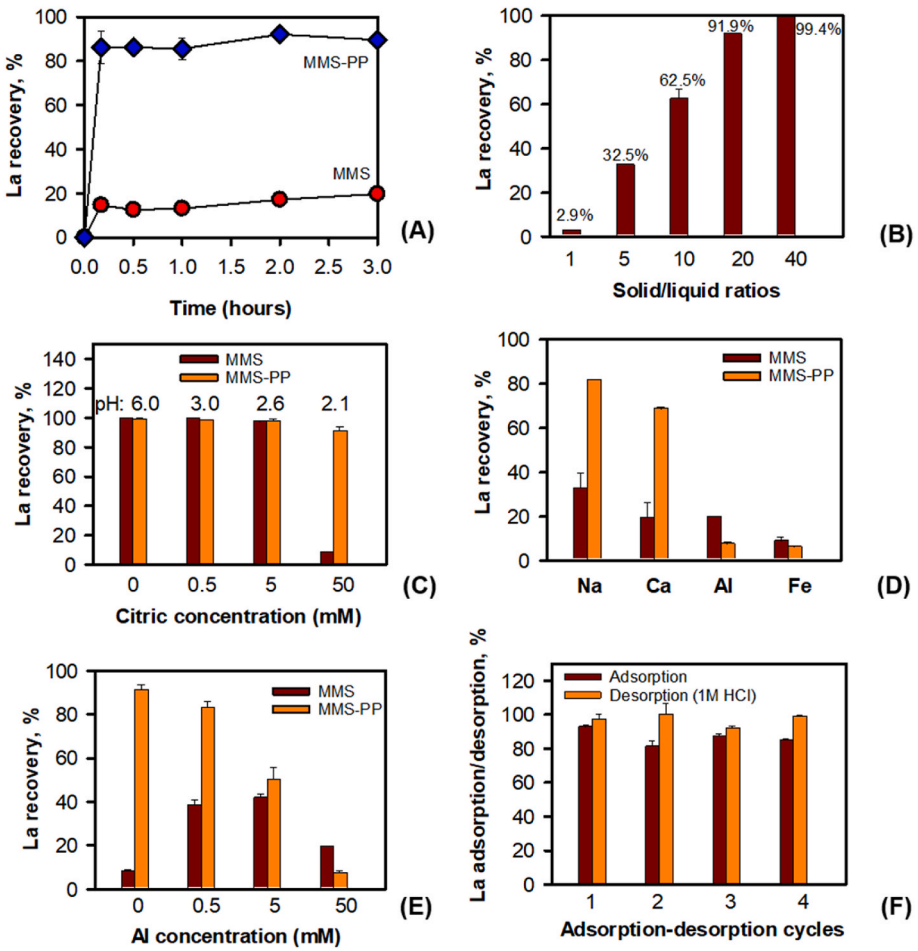

Fig. 3. Effects of other factors on La recovery from 50 mM citric acid simulant by MMS-PP in comparison with MMS. If not specified, reaction conditions are 24 h, solid/liquid ratio 10 g/L, and initial La concentration 0.5 M. **(A)** Reaction time, **(B)** Solid/liquid ratio (30 min, initial La concentration 1.25 mM), **(C)** Citric concentration, **(D)** Competing cations Na^{+}, Ca^{2+}, Al^{3+}, and Fe^{3+}, each at 50 mM, **(E)** Al^{3+} concentrations, and **(F)** Adsorption-desorption cycles (30 min, 1 M HCl for desorption).

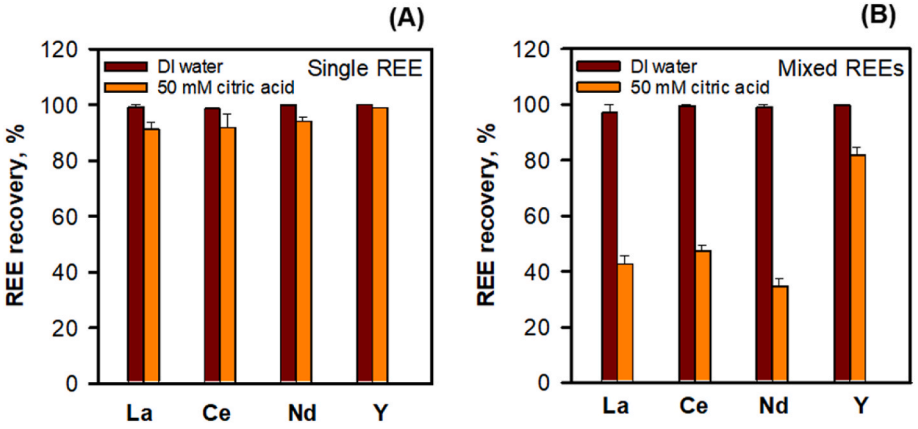

Fig. 4. Recovery comparison of La, Ce, Nd and Y from DI water and 50 mM citric acid simulant by MMS-PP (reaction condition: 24 h, and solid/liquid ratio 10 g/L). **(A)** Single REE, each at an initial concentration of 0.5 M, **(B)** Mixed REEs, each at an initial concentration of 0.5 M.

2 from the propyl chain, and the peak at 7.3 ppm is from carbon 3 (C-Si) (Hernández-Velázquez et al., 2019). The ^{31}P CPMAS NMR spectrum of MMS-PP is shown in Fig. 1E, where the principal peak for phosphonate was at 30.0 ppm chemical shift, with two spinning side bands at around 100 and -40 ppm (Hernández-Velázquez et al., 2019). Both ^{13}C and ^{31}P NMR spectra of the MMS-PP demonstrated that 3-(trihydroxysilyl) propyl methylphosphonate was grafted onto mesoporous silica and MMS.

3.2. La recovery capacity

The adsorption isotherms of La onto MMS-PP and MMS from DI

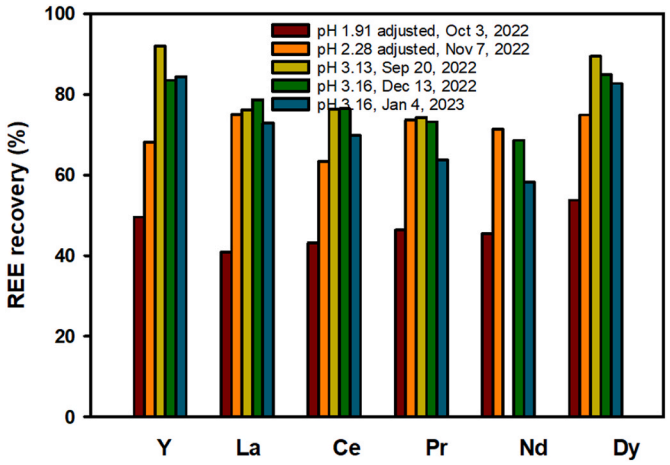

Fig. 5. REEs (Y, La, Ce, Pr, Nd, and Dy) recovery efficiencies from the real citrate extraction solution of MSWI ash by MMS-PP against the solution pH values and storage time.

water (pH ~6.0, Fig. 2A) and 50 mM citric acid simulant (pH ~2.1, Fig. 2B) are shown in Fig. 2. The isotherm data for MMS-PP were analyzed using the Langmuir isotherm model (Equation (3)) to obtain the maximum adsorption capacity values (q_{max}) by plotting C_{eq}/q_{eq} versus C_{eq} (Fig. 2C).

$$\frac{C_{eq}}{q_{eq}} = \frac{1}{q_{max}} C_{eq} + \frac{1}{K_L q_{max}} \quad (3)$$

where q_{eq} is the mass of La sorbed onto the sorbent at equilibrium, q_{max} is the saturation sorption capacity, C_{eq} is the La concentration in solution at equilibrium, and K_L is the Langmuir constant that is directly related to the binding site affinity. The functionalization of phosphonate onto MMS significantly improved the adsorption of La onto the MMS material. The La adsorption capacity of MMS-PP increased from DI water (pH 6) relative to that from 50 mM citric acid simulant (pH 2.1). The maximum adsorption capacity of La onto MMS-PP from DI water 31.2 mg/g from DI water, compared to ~7.0 mg/g for La onto MMS, while the maximum adsorption capacity of La onto MMS-PP from 50 mM citric acid simulant was 13.3 mg/g, compared to ~2.5 mg/g for La onto MMS.

The La recovery capacity obtained for MMS-PP were compared with the maximum adsorption capacities of REEs on functionalized mesoporous silica materials from literature in Table 1. The La recovery capacities obtained in this work were similar to those of REEs onto hybrid mesoporous silica materials reported in some references (Hu et al., 2017, 2019; Yantasee et al., 2009). However, it is noted that several recent studies reported higher sorption capacities for REEs onto other functionalized mesoporous silica materials (Ravi et al., 2018a; Salih et al., 2021; Florek et al., 2015; Zheng et al., 2015, 2020a; Liu et al., 2019; Yin et al., 2020; Lee et al., 2019; Zhang et al., 2017). The discrepancy of the REE adsorption capacities reported between this work and other studies is likely related to pore sizes of the used mesoporous silica, selected organic ligands, and the tested conditions. As expected, the larger pore size of mesoporous silica contributes to higher REE adsorption capacity. Meanwhile, for the same material, higher REE adsorption capacity is achieved under a less acidic pH condition, which is consistent with Fig. 2.

We also synthesized a series of other functionalized MMS materials for La recovery from a citrate simulant and REE recovery from a real citrate extract of MSWI ash (**Text S2** and Fig. S1). These materials were prepared using the same MMS substrate material, but with different functional organic ligands (*e.g.*, benzoylthiourea (BT), dihydroimidazole (DIM), polyaryloamidoxime (AD), phosphonate-amino (PPA), poly (propylenimine) (PPI) dendrimer, poly(amidoamine) (PAMAM) dendrimer, or polyethyleneimine (PEI)) (Li et al., 2016). Our results demonstrated that MMS-PP material was outstanding among all functionalized MMS materials for La recovery from 50 mM citric acid simulant (Fig. S1) or for REE (*i.e.*, Y, La, Ce, Pr, Nd, and Dy) recovery from a real citrate extract of MSWI ash (Fig. S3). The high Gd^{3+} adsorption capacities of amino-phosphonate-functionalized hollow mesoporous silica (Yin et al., 2020) and poly(amidoamine) dendrimer) functionalized mesoporous silica foam (Lee et al., 2019) were likely due to their high surface areas (Table 1). Thus, functionalizing phosphonate onto other mesoporous silica such as SBA-15 or KIT-6 is expected to substantially improve the REE recovery efficiency from the real citrate extracts of MSWI ash, which requires future research to confirm.

3.3. Effects of other factors on La recovery

Batch experiments were conducted to evaluate the effects of reaction time, solid/liquid ratio, citric acid concentration (pH), competing cations (Na^+, Ca^{2+}, Al^{3+} and Fe^{3+}), and adsorption-desorption cycles on La recovery by MMS and MMS-PP from citric acid simulant (Fig. 3). The La adsorption reactions by both MMS and MMS-PP reached steady state within 10 min, and MMS-PP displayed significantly higher La recovery efficiency (>80% vs. ~20%) (Fig. 3A). The La recovery rate by MMS-PP from the 50 mM citric acid simulant increased with increasing solid/liquid ratio (Fig. 3B). With an initial La concentration of 1.25 mM, a MMS-PP loading at the solid/liquid ratio of 40 allowed a nearly 100% La recovery.

The effect of citric acid concentration or solution pH on La recovery is shown in Fig. 3C. Increasing citric acid concentration from 0 to 5 mM in the simulants decreased the solution pH from 6.0 to 2.6. The La recovery at remained high at 97.4% and 99.8% for MMS and MMS-PP materials. Increasing citric acid concentration to 50 mM (pH 2.1) in the simulant led to a significant decrease of La recovery to 8.5% for MMS. At this pH, the surface charge of MMS is near zero or slightly positive, as the isoelectric point of mesoporous silica such as SBA-15 is pH 2.3, (Calzada et al., 2019; Zheng et al., 2020b; Puziy et al., 2007) so the electrostatic attraction between MMS and trivalent La cation is weaker compared to a higher pH, at which the MMS surface is negatively charged. In contrast, MMS-PP still recovered 91.2% of La from the 50 mM citric acid simulant, thanks to the strong binding of La to functionalized phosphonate groups on MMS-PP. These results showcase the superior uptake efficiency of La by MMS-PP from acidic to near-neutral condition compared to MMS.

There is generally an excess of competing metal cations in real extraction solutions due to the unselective leaching processes, which might significantly interfere the selective recovery of La and other REEs. The impacts of Na^+, Ca^{2+}, Al^{3+}, and Fe^{3+} (major cations at high concentrations in the extraction solution of MSWI ash, Table S1) on La recovery by MMS and MMS-PP materials were investigated in 50 mM citric acid simulant (Fig. 3D). The concentration of each competing cation (50 mM) was 100 times that of La (0.5 mM) in the simulant. For both MMS and MMS-PP, the La recovery percentage decreased in the presence of Na^+ and Ca^{2+}, but more significantly for Al^{3+} and Fe^{3+}. The stronger inhibitory effect of Al^{3+} and Fe^{3+} is expected because they carry the same charges as La^{3+} and could compete for binding sites on MMS or MMS-PP surfaces. Similar observation has also been reported by a previous study on REE adsorption by functionalized silica particles that trivalent cations (e.g., Al^{3+} and Fe^{3+}) showed a stronger impeding impact than divalent cations (e.g., Ca^{2+}, Mg^{2+}, and Zn^{2+}), especially at elevated concentrations (Callura et al., 2018). Fig. 3E shows the effect of Al^{3+} concentrations on La recovery efficiency from 50 mM citric acid simulant. For MMS, the La recovery efficiency increased initially with increasing Al^{3+} concentration, and afterward decreased at the 50 mM Al. For MMS-PP, the La recovery efficiency decreased as the Al^{3+} concentration increased to 50 mM. The effect of Fe^{3+} concentrations on La recovery efficiency was similar to that of Al^{3+} (Fig. S2). These results indicate that the selectivity of MMS-PP material toward La is good against Na^+ and Ca^{2+}, but just moderate against Al^{3+} and Fe^{3+}. To

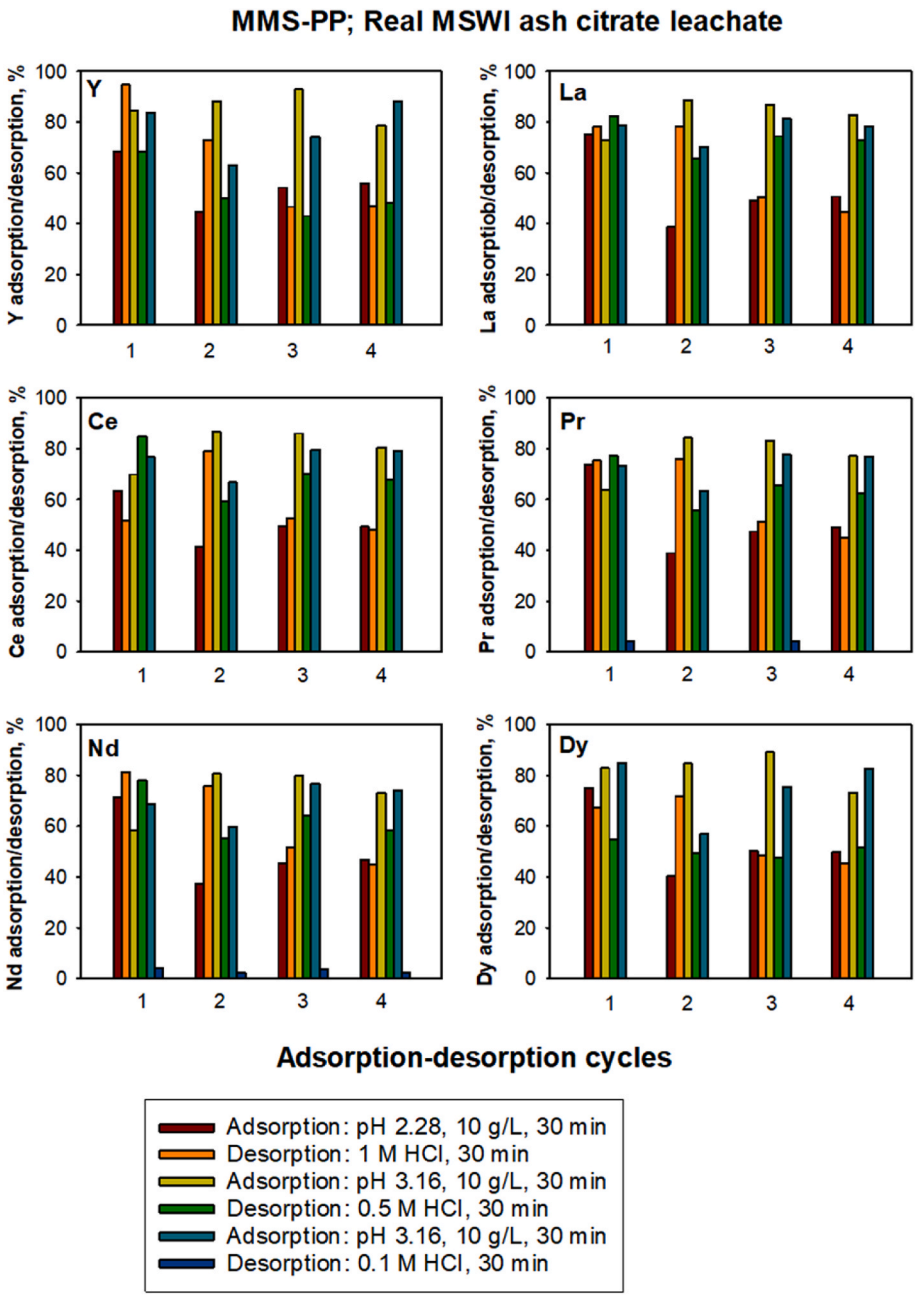

Fig. 6. REEs (*i.e.*, Y, La, Ce, Pr, Nd, and Dy) recovery and desorption efficiencies from the real citrate extraction solution of MSWI ash by MMS-PP. Adsorption conditions: 30 min, solid/liquid ratio 10 g/L. Desorption conditions: 30 min, HCl striping solutions of 0.1, 0.5, or 1 M.

secure a high selectivity towards La, pretreatment processes such selective precipitation might be needed to reduce the concentrations of Al and Fe in the extraction solution prior to MMS-PP sorption (Liu et al., 2023).

The La adsorption/desorption behaviors by MMS-PP were investigated by using 1 M HCl solution as a stripping agent. Over the four adsorption-desorption cycles, the La recovery efficiency by MMS-PP remained at 82–93% from the 50 mM citric acid simulant with an initial La concentration of 0.5 M, and the La desorption efficiency from MMS-PP remained at 92–100% (Fig. 3F). These results show that the MMS-PP material can be regenerated and reused for La recovery from the citric acid extraction solution for at least four times, and La can be readily desorbed and concentrated by 1 M HCl stripping solution, indicating a high recyclability.

3.4. Comparison of La, Ce, Nd and Y recovery from simulants

La, Ce, Nd and Y are the four major REEs with the highest concentrations in MSWI ash based on our preliminary analysis (Table S1). Two batch experiments were conducted to evaluate if the MMS-PP material is also effective for Ce, Nd, and Y recovery. Fig. 4A shows La, Ce, Nd, or Y recovery efficiency for a single REE with an initial concentration of 0.5 M in DI and 50 mM citric acid simulant. The La, Ce, Nd, and Y recovery efficiency was 98.5–99.9% from DI water, and 91.2–98.8% from 50 mM citric acid simulant. Fig. 4B shows La, Ce, Nd, or Y recovery percentage from DI and 50 mM citric acid simulant in which the four REEs coexisted with an initial concentration of 0.5 M for each REE. With a total REE concentration of 2 M, the La, Ce, Nd, and Y recovery efficiency by MMS-PP reached 96.9–99.7% from DI water, but varied from 34.5% (Nd), 42.5% (La), 47.2% (Ce), to 81.7% (Y) from 50 mM citric acid

simulant due to saturation effect. Interestingly, sorption by MMS-PP exhibited a fractionation trend towards Y over La, Ce, and Nd, which could have important implications for separating light and heavy REE. The results demonstrated that the MMS-PP material is effective for REE recovery from citric acid simulant, especially for Y, and can be potentially utilized for La and other REE recovery from citric acid extraction solution of MSWI ash.

3.5. MMS-PP material for REE recovery from a real citrate extract of MSWI ash

MMS-PP was also evaluated for REE (*i.e.*, Y, La, Ce, Pr, Nd, and Dy) recovery from a real citrate extract of MSWI ash (Table S1) in comparison with non-functionalized MMS and several other functionalized MMS materials (Fig. S3). The results illustrate the outstanding performance of MMS-PP among these MMS materials, with REE recovery efficiencies of 80–95% from the real citrate extract. MMS-PP was further evaluated for REE recovery from the real citrate extract against different solution pH values and storage times of extraction solution (Fig. 5). The results show that at pH 1.91, REE recovery by MMS-PP was at 40–50%, which increased to 70–95% at pH 2.28–3.16. The pH values of the real citrate extraction solution were stable at 3.13–3.16 during nearly four-month storage, and the REE recovery efficiencies of MMS-PP also remained at 70–95%.

The MMS-PP material was evaluated for REE (*i.e.*, Y, La, Ce, Pr, Nd, and Dy) recovery and recycling efficiencies from the real citrate extraction solution over four adsorption-desorption cycles. As shown in Fig. 6, at pH 2.28, REE recovery efficiencies were 65–80% for the first cycle but decreased to 40–55% for the subsequent cycles; whereas at pH 3.16, the REE recovery efficiencies remained at 65–85% over four cycles. For REE recycling or desorption, a 0.1 M HCl striping solution was not effective and only desorbed 0–5% REE for each of the four cycles. Increasing the HCl concentration to 0.5 and 1 M was markedly more effective in REE stripping (40–80% desorbed). For all these REEs, the recycling efficiencies were higher (70–80%) in the first two cycles and decreased to 40–50% in the last two cycles. Overall, the MMS-PP still demonstrated a decent recyclability over four cycles.

4. Conclusions

In this work, functionalized MMS materials were developed for selective REE recovery from a complex matrix. With such organic-inorganic hybrid materials, magnetite core can facilitate their separation from liquid media, and mesoporous silica exhibits high and tunable surface area and pore size, which can provide high capacity for REE recovery. In addition, functionalization of organic ligands onto mesoporous silica pores can further improve REE recovery capacity and selectivity. Phosphonate-functionalized MMS material was effective for La recovery from 50 mM citric acid extraction simulant, and exhibited fast adsorption reaction, good La selectivity against competing Na^{+} and Ca^{2+}, and robust efficacy over four adsorption-desorption cycles. The MMS-PP material was demonstrated for effective REE (*i.e.*, Y, La, Ce, Nd, Pr and Dy) recovery (70–95%) from real citrate-assisted extraction solution of MSWI ash. The spent MMS-PP material can be regenerated, and REEs can be recycled for at least four adsorption-desorption cycles. This research demonstrated that functionalized mesoporous materials in combination with citrate-assisted extraction can potentially provide a green, effective, and tunable solid-liquid separation platform for REE and other critical metal recovery from complex solid waste streams.

Notes

The authors declare no competing financial interest.

CRediT authorship contribution statement

Dien Li: Conceptualization, Data curation, Formal analysis, Funding acquisition, Investigation, Methodology, Project administration, Resources, Validation, Visualization, Writing – original draft, Writing – review & editing. **Yinghao Wen:** Investigation, Writing – review & editing. **Lei Hu:** Investigation. **Xiaoyu Xu:** Investigation. **Breann S. Spencer:** Investigation. **Shani Egodawatte:** Investigation. **Sarah C. Larsen:** Investigation. **Yuanzhi Tang:** Conceptualization, Data curation, Formal analysis, Funding acquisition, Investigation, Methodology, Project administration, Resources, Supervision, Validation, Visualization, Writing – original draft, Writing – review & editing.

Declaration of competing interest

The authors declare that they have no known competing financial interests or personal relationships that could have appeared to influence the work reported in this paper.

Data availability

Data will be made available on request.

Acknowledgements

This work was supported by the U.S. Department of Energy ARPA-E program under Grant #DE-AR0001394, Department of Defense SERDP Program under Grant # WP22-3463, and National Science Foundation under Grant #2327659. Work conducted at Savannah River National Laboratory was supported under the U.S. Department of Energy Contract DE-AC09-96SR18500. Dr. Xu's participation was supported by the U. S. Department of Energy under Award Numbers DE-FC09-07SR22506 to the University of Georgia Research Foundation.

Appendix A. Supplementary data

Supplementary data to this article can be found online at https://doi.org/10.1016/j.apgeochem.2024.105900.

References

Antonick, P.J., Hu, Z.C., Fujita, Y., Reed, D.W., Das, G., Wu, L.L., Shivaramaiah, R., Kim, P., Eslamimanesh, A., Lencka, M.M., et al., 2019. Bio- and mineral acid leaching of rare earth elements from synthetic phosphogypsum. J. Chem. Thermodyn. 132, 491–496.

Auerbach, R., Bokelmann, K., Stauber, R., Gutfleisch, O., Schnell, S., Ratering, S., 2019. Critical raw materials - advanced recycling technologies and processes: recycling of rare earth metals out of end of life magnets by bioleaching with various bacteria as an example of an intelligent recycling strategy. Miner. Eng. 134, 104–117.

Brewer, A., Dohnalkova, A., Shutthanandan, V., Kovarik, L., Chang, E., Sawvel, A.M., Mason, H.E., Reed, D., Ye, C.W., Hynes, W.F., et al., 2019. Microbe encapsulation for selective rare-earth recovery from electronic waste leachates. Environ. Sci. Technol. 53, 13888–13897.

Callura, J.C., Perkins, K.M., Noack, C.W., Washburn, N.R., Dzombak, D.A., Karamalidis, A.K., 2018. Selective adsorption of rare earth elements onto functionalized silica particles. Green Chem. 20 (7), 1515–1526.

Calzada, L.A., Castellanos, R., García, L.A., Klimova, T.E., 2019. TiO_2, SnO_2 and ZnO catalysts supported on mesoporous SBA-15 versus unsupported nanopowders in photocatalytic degradation of methylene blue. Microporous Mesoporous Mater. 285, 247–258.

Chen, X.Q., Lam, K.F., Yeung, K.L., 2011. Selective removal of chromium from different aqueous systems using magnetic MCM-41 nanosorbents. Chem. Eng. J. 172, 728–734.

Daigle, B., DeCarlo, S., 2021. Rare Earths and the U.S. Electronics Sector: Supply Chain Developments and Trends, Office of Industries Working Paper ID-075. U.S. International Trade Commission.

Datt, A., El-Maazawi, I., Larsen, S.C., 2012. Aspirin loading and release from MCM-41 functionalized with aminopropyl groups via co-condensation or postsynthesis modification methods. J. Phys. Chem. C 116, 18358–18366.

Egodawatte, S., Datt, A., Burns, E.A., Larsen, S.C., 2015. Chemical insight into the adsorption of chromium(III) on iron oxide/mesoporous silica nanocomposites. Langmuir 31, 7553–7562.

Florek, J., Chalifour, F., Bilodeau, F., Lariviere, D., Kleitz, F., 2014. Nanostructured hybrid materials for the selective recovery and enrichment of rare earth elements. Adv. Funct. Mater. 24 (18), 2668–2676. https://doi.org/10.1002/adfm.201303602.

Florek, J., Mushtaq, A., Lariviere, D., Cantin, G., Fontaine, F.G., Kleitz, F., 2015. Selective recovery of rare earth elements using chelating ligands grafted on mesoporous surfaces. RSC Adv. 5 (126), 103782–103789. https://doi.org/10.1039/c5ra21027e.

Fryxell, G.E., Lin, Y.H., Fiskum, S., Birnbaum, J.C., Wu, H., Kemner, K., Kelly, S., 2005. Actinide sequestration using self-assembled monolayers on mesoporous supports. Environ. Sci. Technol. 39 (5), 1324–1331. https://doi.org/10.1021/es049201j.

Fryxell, G.E., Mattigod, S.V., Lin, Y.H., Wu, H., Fiskum, S., Parker, K., Zheng, F., Yantasee, W., Zemanian, T.S., Addleman, R.S., et al., 2007. Design and synthesis of self-assembled monolayers on mesoporous supports (SAMMS): the importance of ligand posture in functional nanomaterials. J. Mater. Chem. 17 (28), 2863–2874. https://doi.org/10.1039/b702422c.

Gao, Q., Xie, J.F., Shao, Y.T., Chen, C., Han, B., Xia, K.S., Zhou, C.G., 2017. Ultrafast and high-capacity adsorption of Gd(III) onto inorganic phosphorous acid modified mesoporous SBA-15. Chem. Eng. J. 313, 197–206. https://doi.org/10.1016/j.cej.2016.12.068.

Gergoric, M., Ravaux, C., Steenari, B.M., Espegren, F., Retegan, T., 2018. Leaching and recovery of rare-earth elements from neodymium magnet waste using organic acids. Metals 8, 721.

Gutiérrez-Gutiérrez, S.C., Coulon, F., Jiang, Y., Wagland, S., 2015. Rare earth elements and critical metal content of extracted landfilled material and potential recovery opportunities. Waste Manag. 42, 128–136.

Hernández-Velázquez, P.I., Gutiérrez-Ortega, H.A., CarbajalArizaga, G.G., Manríquez-González, R., De la Cruz-Hernández, W., Gómez-Salazar, S., 2019. Hybrid functionalized phosphonate silica: insight into chromium removal chemistry from aqueous solutions. J. Mex. Chem. Soc. 63, 130–153.

Honaker, R.Q., Zhang, W., Werner, J., 2019. Acid leaching of rare earth elements from coal and coal ash: implications for using fluidized bed combustion to assist in the recovery of critical materials. Energy Fuels 33, 5971–5980.

Hsu, E., Barmak, K., Westa, A.C., Park, A.A., 2019. Advancements in the treatment and processing of electronic waste with sustainability: a review of metal extraction and recovery technologies. Green Chem. 21, 919–936.

Hu, Y.M., Drouin, E., Lariviere, D., Kleitz, F., Fontaine, F.G., 2017. Highly efficient and selective recovery of rare earth elements using mesoporous silica functionalized by preorganized chelating ligands. ACS Appl. Mater. Interfaces 9 (44), 38584–38593. https://doi.org/10.1021/acsami.7b12589.

Hu, Y.M., Castro, L.C.M., Drouin, E., Florek, J., Kahlig, H., Lariviere, D., Kleitz, F., Fontaine, F.G., 2019. Size-selective separation of rare earth elements using functionalized mesoporous silica materials. ACS Appl. Mater. Interfaces 11 (26), 23681–23691. https://doi.org/10.1021/acsami.9b04183.

Huang, C., Wang, Y.B., Huang, B., Dong, Y.M., Sun, X.Q., 2019. The recovery of rare earth elements from coal combustion products by ionic liquids. Miner. Eng. 130, 142–147.

Kaya, E., Oktar, N., Karakas, G., Murtezaoglu, K., 2010. Synthesis and characterization of Ba/MCM-41. Turk. J. Chem. 34, 935–943.

Kim, D., Powell, L.E., Delmau, L.H., Peterson, E.S., Herchenroeder, J., Bhave, R.R., 2015. Selective extraction of rare earth elements from permanent magnet scraps with membrane solvent extraction. Environ. Sci. Technol. 49, 9452–9459.

Knezevic, N.Z., Slowing, I.I., Lin, V.S.Y., 2012. Tuning the release of anticancer drugs from magnetic iron oxide/mesoporous silica core/shell nanoparticles. Chempluschem 77, 48–55.

Lazo, D.E., Dyer, L.G., Alorro, R.D., Browner, R., 2018. Treatment of monazite by organic acids II: rare earth dissolution and recovery. Hydrometallurgy 179, 94–99.

Lee, Y.R., Zhang, S., Yu, K., Choi, J., Ahn, W.S., 2019. Poly(amidoamine) dendrimer immobilized on mesoporous silica foam (MSF) and fibrous nano-silica KCC-1 for Gd3 + adsorption in water. Chem. Eng. J. 378 https://doi.org/10.1016/j.cej.2019.122133.

Li, D., Egodawatte, S., Kaplan, D.I., Larsen, S.C., Serkiz, S.M., Seaman, J.C., 2016. Functionalized magnetic mesoporous silica nanoparticles for U removal from low and high pH groundwater. J. Hazard Mater. 317, 494–502. https://doi.org/10.1016/j.jhazmat.2016.05.093. Article.

Lin, Y.S., Haynes, C.L., 2009. Synthesis and characterization of biocompatible and size-tunable multifunctional porous silica nanoparticles. Chem. Mater. 21, 3979–3986.

Liu, E.X., Chen, L., Dai, J.D., Wang, Y.Y., Li, C.X., Yan, Y.S., 2019. Fabrication of phosphate functionalized chiral nematic mesoporous silica films for the efficient and selective adsorption of lanthanum ions. J. Mol. Liq. 277, 786–793. https://doi.org/10.1016/j.molliq.2019.01.032.

Liu, P., Zhao, S., Xie, N., Yang, L., Wang, Q., Wen, Y., Chen, H., Tang, Y., 2023. Green approach for rare earth element (REE) recovery from coal fly ash. Environ. Sci. Technol. 57 (13), 5414–5423.

Ma, J.X., Wang, Z., Shi, Y., Li, Q., 2014. Synthesis and characterization of lysine-modified SBA-15 and its selective adsorption of scandium from a solution of rare earth elements. RSC Adv. 4 (78), 41597–41604. https://doi.org/10.1039/c4ra07571d.

Makanyire, T., Sanchez-Segado, S., Jha, A., 2016. Separation and recovery of critical metal ions using ionic liquids. Advances in Manufacturing 4, 33–46.

Puziy, A.M., Poddubnaya, O.I., Gawdzik, B., Sobiesiak, M., Tsyba, M., 2007. Functionalization of carbon and silica gel by phosphoric acid. Adsorpt. Sci. Technol. 25 (8), 531–542.

Ramasamy, D.L., Repo, E., Srivastava, V., Sillanpaa, M., 2017. Chemically immobilized and physically adsorbed PAN/acetylacetone modified mesoporous silica for the recovery of rare earth elements from the waste water-comparative and optimization study. Water Res. 114, 264–276. https://doi.org/10.1016/j.watres.2017.02.045.

Ravi, S., Lee, Y.R., Yu, K., Ahn, J.W., Ahn, W.S., 2018a. Benzene triamido-tetraphosphonic acid immobilized on mesoporous silica for adsorption of Nd3+ ions in aqueous solution. Microporous Mesoporous Mater. 258, 62–71. https://doi.org/10.1016/j.micromeso.2017.09.006.

Ravi, S., Zhang, S., Lee, Y.R., Kang, K.K., Kim, J.M., Ahn, J.W., Ahn, W.S., 2018b. EDTA-functionalized KCC-1 and KIT-6 mesoporous silicas for Nd^{3+} ion recovery from aqueous solutions. J. Ind. Eng. Chem. 67, 210–218. https://doi.org/10.1016/j.jiec.2018.06.031.

Salih, K.A.M., Hamza, M.F., Mira, H., Wei, Y.Z., Gao, F., Atta, A.M., Fujita, T., Guibal, E., 2021. Nd(III) and Gd(III) sorption on mesoporous amine-functionalized polymer/SiO_2 composite. Molecules 26.

Smith, R.C., Taggart, R.K., Hower, J.C., Wiesner, M.R., Hsu-Kim, H., 2019. Selective recovery of rare earth elements from coal fly ash leachates using liquid membrane processes. Environ. Sci. Technol. 53, 4490–4499.

Vivero-Escoto, J.L., Carboni, M., Abney, C.W., deKrafft, K.E., Lin, W.B., 2013. Organo-functionalized mesoporous silicas for efficient uranium extraction. Microporous Mesoporous Mater. 180, 22–31.

Wen, Y., Hu, L., Boxleiter, A., Li, D., Tang, Y., 2023. Rare earth elements recovery and waste management of municipal solid waste incineration Ash. ACS Sustain. Res. Manag. Published online https://doi.org/10.1021/acssusresmgt.3c00026.

Wu, S.X., Wang, L.S., Zhao, L.S., Zhang, P., El-Shall, H., Moudgil, B., Huang, X.W., Zhang, L.F., 2018. Recovery of rare earth elements from phosphate rock by hydrometallurgical processes - a critical review. Chem. Eng. J. 335, 774–800.

Yantasee, W., Fryxell, G.E., Addleman, R.S., Wiacek, R.J., Koonsiripaiboon, V., Pattamakomsan, K., Sukwarotwat, V., Xu, J., Raymond, K.N., 2009. Selective removal of lanthanides from natural waters, acidic streams and dialysate. J. Hazard Mater. 168, 1233–1238. https://doi.org/10.1016/j.jhazmat.2009.03.004.

Yin, W.Y., Liu, L.Y., Zhang, H.Y., Tang, S., Chi, R., 2020. A facile solvent-free and one-step route to prepare amino-phosphonic acid functionalized hollow mesoporous silica nanospheres for efficient Gd(III) removal. J. Clean. Prod. 243. https://doi.org/10.1016/j.jclepro.2019.118688.

Zhang, F., Lan, J., Zhao, Z.S., Yang, Y., Tan, R.Q., Song, W.J., 2012. Removal of heavy metal ions from aqueous solution using Fe_3O_4-SiO_2-poly(1,2-diaminobenzene) core-shell sub-micron particles. J. Colloid Interface Sci. 387, 205–212.

Zhang, W.Z., Avdibegovic, D., Koivula, R., Hatanpaa, T., Hietala, S., Regadio, M., Binnemans, K., Harjula, R., 2017. Titanium alkylphosphate functionalised mesoporous silica for enhanced uptake of rare-earth ions. J. Mater. Chem. A 5 (45), 23805–23814. https://doi.org/10.1039/c7ta08127h.

Zhao, Y.G., Li, J.X., Zhang, S.W., Wang, X.K., 2014. Amidoxime-functionalized magnetic mesoporous silica for selective sorption of U(VI). RSC Adv. 32710–32717.

Zheng, X.D., Wang, C., Dai, J.D., Shi, W.D., Yan, Y.S., 2015. Design of mesoporous silica hybrid materials as sorbents for the selective recovery of rare earth metals. J. Mater. Chem. A 3 (19), 10327–10335. https://doi.org/10.1039/c4ta06860b.

Zheng, X.D., Song, Z.Q., Liu, E.X., Zhang, Y.Z., Li, Z.Y., 2020a. Preparation of phosphoric acid-functionalized SBA-15 and its high efficient selective adsorption separation of lanthanum ions. J. Chem. Eng. Data 65 (2), 746–756. https://doi.org/10.1021/acs.jced.9b00976.

Zheng, X., Song, Z., Liu, E., Zhang, Y., Li, Z., 2020b. Preparation of phosphoric acid-functionalized SBA-15 and its high efficient selective adsorption separation of lanthanum ions. J. Chem. Eng. Data 65 (2), 746–756.